Synthetic turbulence

A. Juneja, D. P. Lathrop, K. R. Sreenivasan, and G. Stolovitzky
Mason Laboratory, Yale University, New Haven, Connecticut 06520-8286
(Received 18 October 1993)

A family of schemes is outlined for constructing stochastic fields that are close to turbulence. The fields generated from the more sophisticated versions of these schemes differ little in terms of one-point and two-point statistics from velocity fluctuations in high-Reynolds-number turbulence; we shall designate such fields as synthetic turbulence. All schemes, implemented here in one dimension, consist of the following three ingredients, but differ in various details. First, a simple multiplicative procedure is utilized for generating an intermittent signal which has the same properties as those of the turbulent energy dissipation rate ϵ. Second, the properties of the intermittent signal averaged over an interval of size r are related to those of longitudinal velocity increments $\Delta u(r)$, evaluated over the same distance r, through a stochastic variable V introduced in the spirit of Kolmogorov's refined similarity hypothesis. The third and final step, which partially resembles a well-known procedure for constructing fractional Brownian motion, consists of suitably combining velocity increments to construct an artificial velocity signal. Various properties of the synthetic turbulence are obtained both analytically and numerically, and found to be in good agreement with measurements made in the atmospheric surface layer. A brief review of some previous models is provided.

PACS number(s): 47.27.Eq, 47.27.Jv

I. INTRODUCTION

It is now well understood that the inertial and dissipative ranges of scales of turbulent motion at high Reynolds numbers are independent of the flow configuration—at least to a degree that is usefully accurate—and it follows that these scales of motion depend only on a few gross parameters. An important question, then, is as follows: What is the smallest set of parameters which adequately incorporate all the universal aspects of turbulent motion—at least to some reasonable accuracy? In part, this paper is devoted to answering the question. One can construct, with relatively modest physical input, stochastic signals that have most properties of a turbulence velocity trace at high Reynolds numbers. For convenience, artificial signals mimicking real turbulence well will be designated as synthetic turbulence.

One of the relevant observations [1] in this regard is that the longitudinal velocity increments in the inertial range of scales share some of the properties of fractional Brownian motion [2] with a Hurst exponent of about 0.35. However, this is only partially true because the increments of fractional Brownian motion are symmetrically distributed, whereas the turbulent velocity increments have a finite skewness [3]. Several other methods [4–7] can produce signals possessing various properties of turbulence but fall short in some ways. Except for Ref. [4], the models in general do not successfully incorporate the skewness and odd-order structure functions. Indeed, the finite skewness of longitudinal velocity increments is an important property related to energy transfer across scales, and its incorporation into a simple scheme is a major challenge. Another important consideration is the incorporation of small-scale intermittency in the dissipation field obtained from the velocity derivatives.

In this paper, we outline a family of schemes for generating turbulencelike signals that mimic real turbulence to various degrees of detail; in the more refined schemes used here, the signals generated do not differ significantly from real turbulence in the sense of one-point and two-point statistics. All schemes consist of three essential ingredients. First, an appropriate multiplicative procedure is utilized for generating intermittent positive signals (or measures) possessing many of the properties of turbulent energy dissipation, ϵ. The properties of the measure living in a box of size r are then related to those of velocity increments $\Delta u(r)$ over a separation distance r. This is done *via* a stochastic variable V introduced in the spirit of Kolmogorov's refined similarity hypothesis. The third and final step consists of constructing synthetic turbulence by suitably combining the velocity increments.

Following a brief review of previous models in Sec. II, we discuss in Sec. III the broad background needed for constructing synthetic turbulence. In Sec. IV, we discuss some preliminary models for generating artificial velocity fields in order to highlight their drawbacks and motivate the scheme employed for more sophisticated models described in detail in Sec. V. Section VI relates the parameters of the synthetic turbulence model to those of real turbulence by making some analytical predictions from the model. This section also includes an analytical prediction of derivative skewness for synthetic turbulence. Section VII contains a comparison of the properties of synthetic turbulence with those of velocity fluctuations measured in the atmospheric boundary layer a few meters above the ground. The properties examined include power spectral density, the fractal dimension, Kolmogorov's refined similarity hypotheses, the scaling of odd- and even-order structure functions up to the eighth order, and the multifractal scaling of ϵ_r constructed from synthetic tur-

1063-651X/94/49(6)/5179(16)/$06.00

bulence. The agreement with measurements is found to be very good. The results are summarized in Sec. VIII.

II. SOME PREVIOUS MODELS

We now present a brief review of some previous models proposed in recent literature for constructing signals which share some properties of turbulent velocity fluctuations. While all of these models yield the correct form for even-order structure function exponents, they fail (except for Ref. [4]) to incorporate the skewness of velocity increments, and odd-order structure functions in general. Further, some of them do not incorporate small-scale intermittency and do not satisfy the continuous scale symmetry imposed by the Navier-Stokes equations in the inertial range, nor do they satisfy the continuous translational invariance necessary to model homogeneous turbulence.

Eggers and Grossmann [4]. These authors propose a one-dimensional model for the turbulent velocity field using a Fourier-Weierstrass basis. The model consists of a superposition of successively smaller eddies forming a Cayley-tree-like structure. The model is written as

$$u(x)=\sum_{l=-N_\eta}^{N_L} u^{(l)}(x)e^{i\lambda^{-l}x/L_0}+\text{c.c.}\ , \tag{1}$$

where L_0 is a reference length scale, $\lambda>1$ is real scaling factor, $u^{(l)}(x)$ represents the amplitude of an eddy of level l at position x, and c.c. stands for the conjugated complex. The randomness of eddy decay is modeled by a multiplier distribution similar in spirit to that of the p model (see below), which forms the $u^{(l)}$ amplitudes. The authors study the influence of physical assumptions of the cascade (spatial coherence of eddies and a version of viscous cutoff) on the intermittency exponent which determines the behavior of the scaling of structure functions. Of the four papers summarized here, this is the only one which addresses the issue of skewness.

Humphrey, Schuler, and Rubinsky [5]. These authors propose a deterministic multifractal Weierstrass-Mandelbrot function to represent dissipative as well as inertial range scales of turbulence

$$u_F(t)=\sum_{j=1}^{m} A_j \sum_{n=n_{1j}}^{n_{2j}} \frac{\sin(\omega t)}{\omega^{H_j}}\ . \tag{2}$$

Here, $\omega=b^n$ where b is a constant (~ 1), $b^{n_{2m}}$ and $b^{n_{11}}$ are the largest and smallest frequencies in the series, and A_j and H_j are scale independent constants with the constraint $0<H_j<1$. They show that this representation yields correct forms for energy and dissipation spectra for fully developed turbulence in various flows.

Vicsek and Barabasi [6]. The authors propose a multiaffine model to represent the turbulent velocity fluctuations. The model makes use of a generator function which takes the form of an asymmetrical z made of three intervals. At each step of the iterative procedure, the intervals obtained in the previous step are replaced with properly rescaled version of the generator or its mirror image. The authors find good agreement with experimental data for velocity structure functions and generalized dimensions for velocity derivatives.

Benzi et al. [7]. Using information about the scaling exponents of structure functions, the authors propose a generalization of the recursive scheme to generate, *via* self-affine functions, a multiaffine field resembling velocity fluctuations in turbulent flows. The authors also provide an alternative interpretation of their scheme in terms of a wavelet decomposition. In particular, the one-dimensional velocity field is given by

$$\Phi(x)=\sum_{j=-\infty}^{+\infty}\sum_{k=-\infty}^{+\infty} \alpha_{j,k}\psi_{j,k}(x)\ , \tag{3}$$

where $\psi_{j,k}(x)=2^{j/2}\psi(2^j x-k)$, $\psi(x)$ being a basis function with zero mean, and $\alpha_{j,k}$ are a set of coefficients forming a dyadic structure. The authors point out that the scheme can be generalized to three dimensions, and study the probability distribution functions of the increments of the signal.

While each of these schemes is ingenious in its own way and succeed to varying degrees, their salient feature (except for Ref. [4]) is that they are based on mathematical constructs providing little insight into the underlying physics. The significant difference of the schemes described in this paper is that they are based more firmly in turbulence physics, as revealed from both classical and more recent work. The physical content of Ref. [4] is somewhat similar to that used here, but our schemes for constructing the velocity signal are conspicuously different, mainly because we incorporate continuous scale invariance in the inertial range as well as continuous translational symmetry.

III. BACKGROUND

A. The p model for the energy dissipation

One of the central physical quantities in turbulence is the energy dissipation rate. Its definition

$$\bar{\epsilon}=\tfrac{1}{2}\nu\sum_{i,j}\left[\frac{\partial u_i}{\partial x_j}+\frac{\partial u_j}{\partial x_i}\right]^2 \tag{4}$$

involves the spatial derivatives of the three components of the velocity. In Eq. (4), ν is the kinematic viscosity of the fluid, and u_k ($k=1,2,3$) represents the component of the velocity vector in the direction x_k. It is often convenient to deal with the one-dimensional surrogate of the above equation, namely,

$$\epsilon=15\nu\left[\frac{\partial u}{\partial x}\right]^2\ , \tag{5}$$

where u is the x component of the velocity. We shall follow this practice designating ϵ itself as the energy dissipation rate. The intermittent nature of ϵ has been described relatively successfully by means of a multifractal formalism, e.g., Refs. [8] and [9]. The quantity of basic interest in building up a multifractal measure is the so-called multiplier distribution [10]. [For our purposes, a measure is any positive definite quantity which is additive in the

sense that the quantity summed over two nonoverlapping intervals equals the sum of that quantity over the two intervals. Here, the total dissipation rate contained in the segment $[x,x+r]$ is equal to $r\epsilon_r(x,t)=\int_x^{x+r}dx\,\epsilon(x)$ is the appropriate measure for that interval. Note that the meaning of $\epsilon_r(x)$ is the local average of ϵ in the segment $[x,x+r]$.] The multiplier distribution is the probability density of the multiplier M, which is the ratio of the measure inherited by an offspring piece to that contained in the parent piece. That is, if one divides an interval of size r into two equal (nonoverlapping) pieces of size $r/2$, one of the latter pieces contains a fraction M of the parent measure, and the other piece contains the fraction $1-M$. Now, M is a random variable for turbulence, possessing a well-defined probability density function (PDF), which is invariant in the inertial range [10]. From this scale-invariance emerge all the multifractal scaling properties of the energy dissipation, observed in a variety of fully developed turbulent flows [9].

It has been shown in Ref. [11] subsequently that a variety of simple quasideterministic models can be constructed from the measured multiplier distribution. The simplest among them is the so-called p model of Ref. [12]. In the one-dimensional version of the p model, an interval of size r breaks down into two subintervals of equal size $r/2$, and a fraction p of the measure contained in the parent interval is inherited by one piece (either the left or the right with equal probabilities) and a fraction $1-p$ by the other piece. This process is repeated with fixed p, until one reaches scales of size η, where $\eta=(\nu^3/\langle\epsilon\rangle)^{1/4}$ is known as the Kolmogorov scale. Using results from the multifractal analysis of experimentally obtained dissipation data, it was found in Ref. [12] that a p model with $p=0.7$ and $1-p=0.3$ yields an intermittent measure which exhibits the same statistical properties as the one-dimensional surrogate of turbulent energy dissipation. Figure 1 illustrates the procedure for constructing the dissipation signal $d(x)$ on a unit interval ($x\in[0,1]$) according to the p model. The p model is equivalent to prescribing the multiplier distribution as

$$P(M)=\frac{\delta(M-p)+\delta(M-[1-p])}{2}\ . \tag{6}$$

The p model is one of the ingredients we shall use to construct the velocity signal. It should be emphasized, however, that a number of different dynamical processes can yield the same multifractal spectrum for dissipation, and that the p model is representative of a class of models which agree with experimental data. Its simplicity and good agreement with experiments make it a useful model; the real process is evidently far more complex.

B. The l model for the energy dissipation

Like the p model described earlier, the so-called l model [13] also employs a multiplicative procedure for generating an intermittent measure resembling the turbulent energy dissipation. In the one-dimensional version of this model, a scale of size r breaks up into two subscales of sizes r_1 and r_2, which are generally unequal and are such that the measure contained in each offspring is equal to half the measure contained in the parent scale. Just as before, underlying the multiplicative process is a multiplier distribution for the lengths of the offspring pieces. The PDF of the multipliers ($l_1=r_1/r$ and $l_2=l-l_1=r_2/r$) was computed from the experimentally obtained turbulent energy dissipation. Its shape is essentially independent of the scale r in the inertial range (Fig. 2). Note that the dissipation contained in any scale at level n of the cascade is simply $(\frac{1}{2})^n L\epsilon_0$ and the size of the eddy is equal to $[\prod_{i=1}^n l_i]L$, where $L\epsilon_0$ is the dissipation contained in the largest eddy L and the l_i's ($0<l_i<1$) represent the multipliers.

Following the procedure laid out in [11], similar to the case of the p model, one can determine a quasideterministic approximation to the probabilistic process represented by the multiplier distribution in Fig. 2. This model turns out to have the following feature: Split an interval of size r into two unequal intervals in the ratio of 0.7 and 0.3, and assign to each of them half the measure contained in the original interval. Unlike the p model, the scales at a given level n are not all equal, but the average length scale is equal to $L2^{-n}$. Repeat this procedure until the smallest average scale is equal to the Kolmogorov scale. Figure 3 illustrates a few stages in the construction of the l-model dissipation rate.

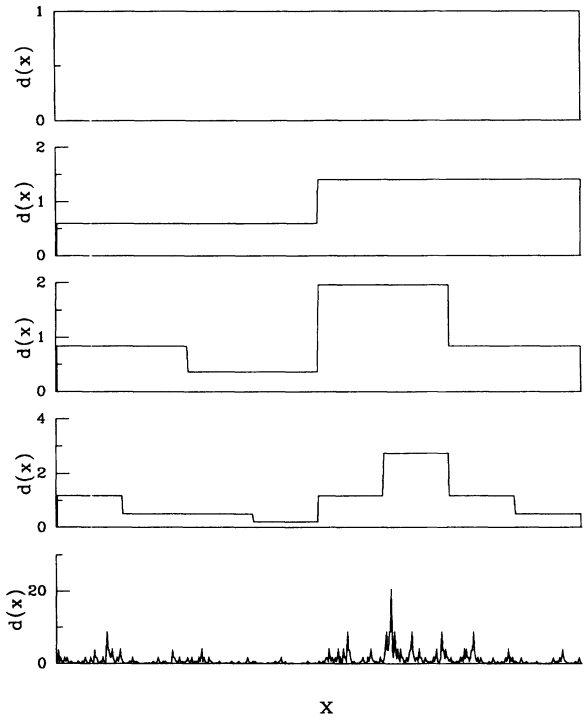

FIG. 1. The p model for generating an intermittent measure $d(x)$ on a unit interval ($x\in[0,1]$) employs unequal multipliers ($p_1=0.7$ and $p_2=0.3$) to refine an initially uniform measure according to a binary scheme. The outcome of the first three steps and that at the end of nine steps are shown.

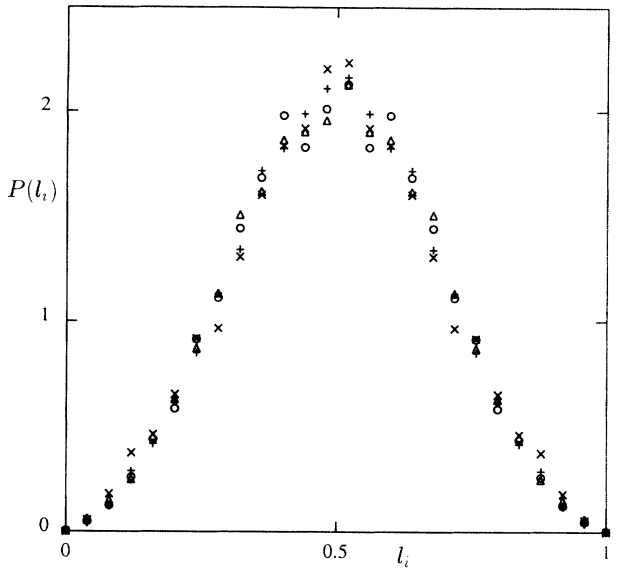

FIG. 2. The probability density function of length multipliers l_i obtained from atmospheric turbulence velocity data. Many intervals of a certain size chosen in the inertial range are each split into two parts such that the measure in each offspring piece is equal to half that in the parent piece. The distribution of the ratio of the offspring pieces to that of the parent piece is obtained. Different symbols correspond to different initial lengths in the inertial range: △ at 32η, ○ at 64η, + at 128η, and x at 256η, η being the measured Kolmogorov scale.

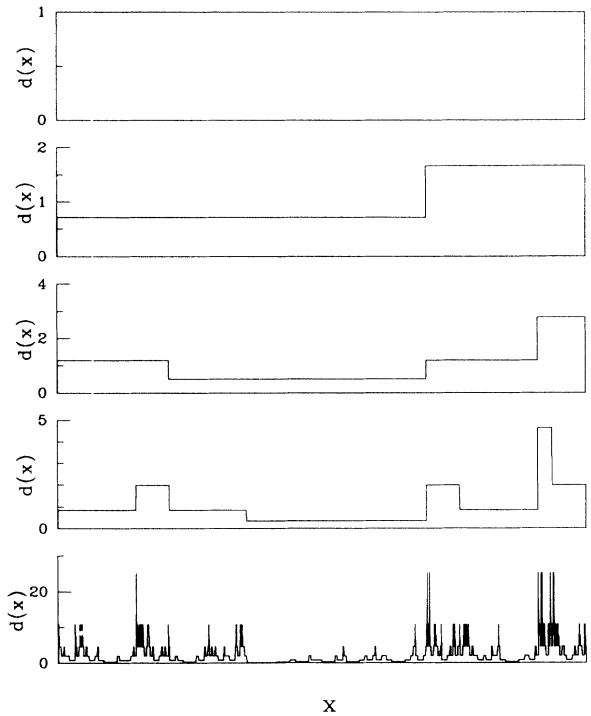

FIG. 3. The l model for generating an intermittent measure $d(x)$ on a unit interval ($x \in [0,1]$) redistributes equal measure on unequal length scales at each stage of the construction. Unequal multipliers ($l_1=0.7$ and $l_2=0.3$) are employed to determine the length scales at the next step of the cascade. (These specific values of multipliers were chosen according to the method proposed in Ref. [11]). The outcome of the first three steps and that at the end of nine steps are shown.

C. Kolmogorov's refined similarity hypotheses

The energy dissipation rate is an important physical quantity, but of more direct interest in turbulence is the velocity field itself. To relate the energy dissipation rate to the velocity field, one can make use of Kolmogorov's refined similarity hypotheses [14] and convert the dissipation rate into a velocity increment. The hypotheses relate the probability distribution function (PDF) of velocity increment $\Delta u(r)=u(x+r)-u(x)$ to the dissipation rate in the segment $[x,x+r]$, namely $r\epsilon_r(x,t)$. Defining a velocity scale at (x,t) by $U_r=(r\epsilon_r)^{1/3}$ and a local Reynolds number $\mathrm{Re}_r=rU_r/\nu$, the first refined similarity hypothesis states that for $r \ll L$ (L being the integral scale of turbulence)

$$\Delta u(r)=V_{\mathrm{RSH}}(r\epsilon_r)^{1/3}, \tag{7}$$

where V_{RSH} is a stochastic variable whose PDF depends only on Re_r. The second refined similarity hypothesis (RSH) states that, if $\mathrm{Re}_r \gg 1$, the PDF of V_{RSH} becomes independent also of Re_r, this being the spirit of universality.

For quite some time, the relation between the energy dissipation rate and velocity increments has been treated merely as a dimensional relation of the form $|\Delta u(r)| \sim (r\epsilon_r)^{1/3}$. Recently, however, various aspects of the refined similarity hypotheses have been explored in detail [15]. Using data from high-Reynolds-number turbulence in the atmospheric boundary layer, Stolovitzky, Kailasnath, and Sreenivasan [15] studied the properties of the stochastic variable $V_{\mathrm{RSH}}=\Delta u(r)/(r\epsilon_r)^{1/3}$, conditioned on $r\epsilon_r$. They found that for r in the inertial range, the PDF of the stochastic variable V_{RSH} is independent of r and ϵ_r, essentially confirming the universality embodied in the second refined similarity hypothesis. (The refined similarity hypotheses as stated above have some shortcomings in the dissipative range, but it is not central to our immediate purposes.)

The refined hypotheses do not prescribe the precise form of this universal distribution, but a few related statements can be made. First, consistency with Kolmogorov's $\frac{4}{5}$th law [3] demands that $\langle V_{\mathrm{RSH}}^3 \rangle = -0.8$ in the inertial range. That is, the distribution of V_{RSH} is not symmetric. Second, by invoking the fact that velocities separated by distances of the order L are essentially independent of each other, one can write $\langle \Delta u(L)^2 \rangle = 2\langle u^2 \rangle$, where $\langle u^2 \rangle$ is the mean-square turbulence velocity. Further, recalling the result [16] that $\langle \epsilon \rangle = A\langle u^2 \rangle^{3/2}/L$ (with $A \sim 1$ for high enough Reynolds numbers [16]), it follows that the variance of V_{RSH} for $r \sim L$ is approximately 2. Since the universality of V_{RSH} is supposed to extend over the entire range of scales between L and η, the variance $\langle V_{\mathrm{RSH}}^2 \rangle$ can be expected to be 2 in the entire inertial range. (For the sake of simplicity, we are stretching in this argument the validity of the inertial range physics all the way up to L.) The skewness of V_{RSH} is thus of the order of -0.28, which is in good agreement with experimental measurements. Further, this finite (and relatively small) skewness is not concentrated in any particular part of the PDF but is spread

over the entire range of V_{RSH}. The PDF can be fitted well by a distribution close to the Gaussian. One possible form is $V_{\mathrm{RSH}}=\tilde{V}-\langle\tilde{V}\rangle$, where $\tilde{V}$ is distributed according to

$$p(\tilde{V})=N(a)\exp\left[-\frac{\tilde{V}^2}{2\sigma^2}B(\tilde{V},a)\right], \tag{8}$$

with $\sigma^2=2$,

$$B(\tilde{V},a)=\left[1+a\frac{\tilde{V}}{\sigma}\right]\Big/\left[1+\frac{\tilde{V}^2}{\sigma^2}\right]^{1/2}, \tag{9}$$

and $N(a)$ a normalization constant. This expression is motivated by Ref. [17], where it appears in a different context. The PDF of $\tilde{V}-\langle\tilde{V}\rangle$ is a good fit to the measured PDF of V_{RSH}, and yields the right skewness when $a=0.3$.

Finally, it is useful to note that when the largest scales of the velocity of the order L are removed by high-pass filtering, the velocity increments of the remainder are essentially unskewed. It is therefore expected that the variable V_{RSH} computed from the high-pass-filtered velocity is also symmetric, implying that the skewness of V_{RSH} is not an intrinsic property of turbulence in the inertial and dissipative scales. As we shall see, this important factor will be invoked in subsequent work in constructing synthetic turbulence.

D. Fractional Brownian motion

We have so far described two main ingredients of synthetic turbulence, namely, the construction of a measure similar to energy dissipation rate and, from it, the velocity increments in the inertial range. The velocity increments so obtained have to be added together appropriately to produce the velocity signal. It should be emphasized that the increments $\Delta u(r)$ at the smallest r cannot be simply added sequentially because such a procedure yields the classical Brownian motion. Fractional Brownian motion (FBM) is an extension of the Brownian motion to correlated processes [2]. A fractional Brownian motion $X(t)$ is a single-valued function of the variable t, such that its increments $\Delta X(\tau)=X(t_2)-X(t_1)$, $\tau=t_2-t_1$, have a Gaussian distribution with variance

$$\langle[\Delta X(\tau)]^2\rangle\sim\tau^{2H}, \tag{10}$$

where the scaling exponent H is restricted to the range $0<H<1$. The special case with $H=\frac{1}{2}$ is the classical Brownian motion. It is interesting to note that if X is interpreted as one component of turbulent velocity and t as the space coordinate, Eq. (10) defines the second-order structure function.

Fractional Brownian motion has the scaling property [Eq. (10)] that whenever t is scaled by a factor α, X is scaled by α^H. The trace is therefore self-affine. The energy spectrum of a FBM exhibits a $1/f^{\beta}$ dependence. From Eq. (10) and the Wiener-Khintchine relation it follows that the spectral density exponent is related to H through $\beta=2H+1$ [18]. The fractal dimension D of the FBM has been shown [18,19] to be $D=2-H$.

For the Kolmogorov turbulence, there exist certain similarities in the scaling behavior of an FBM with $H=\frac{1}{3}$ and turbulent velocity (see Ref. [1]). An FBM can be generated by combining increments with the required variance at different scales using an additive process [19]. Figure 4 shows an FBM with $H=\frac{1}{3}$ at different stages of construction. The spectral density exponent β for this signal can be verified easily to be about $\frac{5}{3}$. However, the increments for an FBM have a Gaussian distribution (as opposed to turbulence, where the velocity increments have stretched exponential distributions [20]) and are nonskewed by construction. Further, no intermittency is built into the construction because only one scaling exponent is employed. Consequently, high-order structure functions of order m have scaling exponents $m/3$ when m is even and zero when m is odd. To incorporate skewness and small-scale intermittency into a model for constructing synthetic turbulence, more sophisticated alternatives will be necessary. The next sections deal with them.

IV. PRELIMINARY MODELS

The simplest technique for building an artificial velocity field on the basis of the ideas presented in the previous

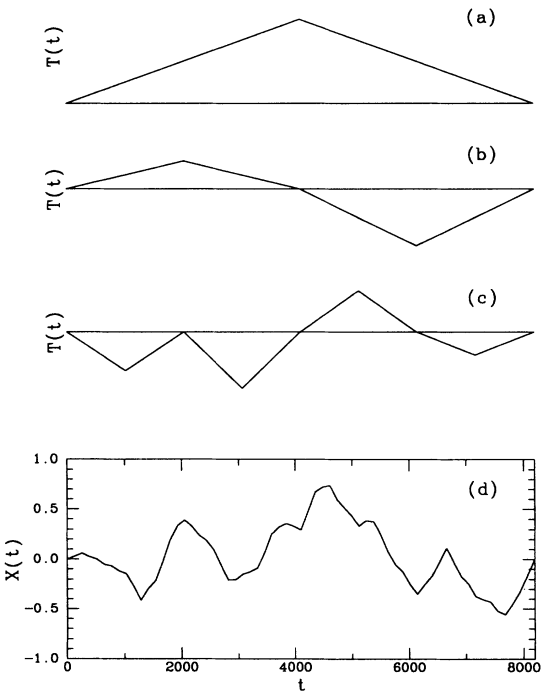

FIG. 4. Construction of fractional Brownian motion using the midpoint addition method. At each successive stage the increment across a scale τ, $\Delta X(\tau)$ [see Eq. (10)] is represented by the amplitude of the tent function $T(t)$, whose base is equal in size to the scale τ. The FBM is formed by superimposing tent functions of all scales (up to some level of refinement), illustrated for the first three steps in (a), (b), and (c); (d) shows the superimposed signal $X(t)$ after eight steps in the construction.

section is as follows. We start by considering an interval of size L on which a measure is uniform and assigned a value of $L\langle\epsilon\rangle$, analogous to the zeroth step in p-model construction. From it, one generates a velocity increment across the scale L in the spirit of Kolmogorov's refined similarity hypotheses, namely, $\Delta u(r) = V(r\epsilon_r)^{1/3}$, $r=L$. The variable V is picked from the appropriate distribution (see below for more details). The interval of size L is next divided into two equal segments (each of length $L/2$) while the measure itself is divided unequally in the ratio 0.7 and 0.3. The measures in these two intervals are again converted to velocity increments across the scales which are equal to half of the original interval. This process is repeated for n number of steps in the p model, at the end of which we have information about velocity increments across various scales at different locations. These scales and locations define the construction at each step of the refinement process.

As in the midpoint addition method for generating fractional Brownian motion (Fig. 4), the velocity increments computed for a given interval can now be interpreted as the amplitudes of symmetric tent functions [Fig. 5(a)] placed on the appropriate intervals. The artificial velocity field is then a straightforward superposition of the tent functions of all scales. We generated signals using the above procedure for two different cases. In one case, the stochastic variable V in Eq. (7) was chosen from a Gaussian distribution; in the second, it was chosen as $\tilde{V}-\langle\tilde{V}\rangle$, where $\tilde{V}$ was picked from a skewed distribution [Eqs. (8) and (9)]. The fields generated for both cases are quite similar to turbulent velocity fields, but suffer from two major drawbacks. First, the power spectrum of the signals exhibits spikes (although the background has the right slope), indicating a lack of continuous scale symmetry. Second, the skewness and other odd-order structure functions are zero even when the variable V is taken from the skewed distribution. In fact, it can be shown analytically that no matter what distribution of V is chosen, a binary cascade model which employs *symmetric* tents cannot yield skewness in the artificial velocity field.

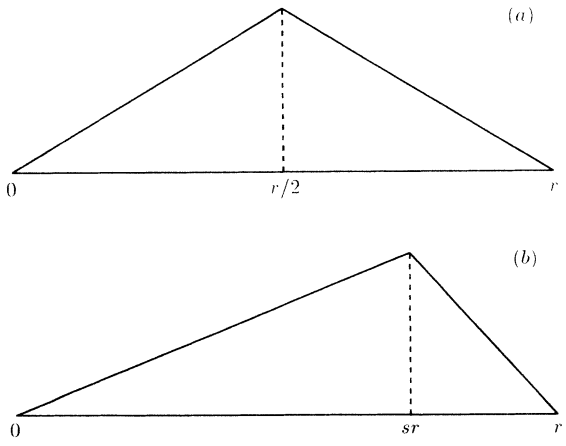

FIG. 5. (a) Symmetric tent function. (b) Skewed tent function.

The appearance of spectral spikes indicates a lack of translational invariance, and is a defect of the model chosen to construct the energy dissipation. In all models of dissipation based on the p model or its several variants, an interval is rigidly divided into two equal parts at each step, which imposes an artificial dyadic grid on to the signal. As mentioned in Sec. III, the p model is only one of the generic possibilities for modeling the energy dissipation. For example, the use of the l model for the dissipation automatically restores translational invariance because one introduces a range of scales at every step of the construction. However, the lack of skewness persists. In order to obtain nonzero skewness, we first note that it is a structural feature that has to be incorporated into a construction scheme explicitly. We turn our attention to a model which employs skewed tents [Fig. 5(b)] instead of symmetric ones. The parameter s in the tent is set at a fixed value different from $\frac{1}{2}$. The other details of the construction remain the same. If the stochastic variable V is chosen from a Gaussian distribution, one does not obtain any skewness in the resulting velocity signal, no matter what value of s is chosen. On the other hand, when V is chosen as $\tilde{V}-\langle\tilde{V}\rangle$, with $\tilde{V}$ picked from the distribution given by Eqs. (8) and (9), it is possible to select the parameter s such that the artificial velocity signal exhibits the right skewness as well as correct scaling for all odd-order structure functions. One way of computing the appropriate value of s will be described in Sec. VI.

The model based on skewed tents and skewed V still possesses two principal drawbacks. As noted already, the use of the p model results in the lack of continuous scale symmetry. Although this problem can be alleviated by using the l model for the energy dissipation, the second problem cannot be so resolved: By using a skewed tent function whose shape remains constant irrespective of the sign of V, one generates a signal which violates the space reversal symmetry of the Navier-Stokes equations (i.e., $x\rightarrow a-x; u\rightarrow -u$ for any a). Hence, if this symmetry is to be preserved, the shape of the tent function *must depend on the sign of stochastic variable V.*

The scope of the remainder of this paper is, therefore, set by the following two considerations. If we choose to use the p model, we need to generate skewed tent functions that are consistent with translational invariance as well as space reversal symmetry. These conditions require that the scale and the location of the skewed tent function be chosen randomly from appropriate continuous distributions. Alternatively, if we choose to use the l model for the energy dissipation, we need not explicitly consider translational invariance (because it is inherent to the l model), but should pay attention to the skewness. The key to both these issues is the generation of a suitable skewed tent function, which will be described below.

V. SYNTHETIC TURBULENCE MODELS

A. Skewed tents of random scales and locations with underlying p model

In this instance, the synthetic turbulence signal will be generated on a unit interval by a superposition of a large

number of localized structures of scales r between $2^{-\alpha_{\max}}$ and $2^{-\alpha_{\min}}$. The unit interval has a resolution of 2^{-n} (i.e., it contains 2^n equispaced points). The parameters $\alpha_{\min}$ and $\alpha_{\max}$ $(0 \le \alpha_{\min} \le \alpha_{\max} \le n)$ will be related in the next section to the integral scale and Reynolds number of the synthetic turbulence being generated. The structures, denoted by $T^{(+)}(x)$ and $T^{(-)}(x)$ (their shape being a function of the sign of their amplitude), take the form of skewed tent functions shown in Fig. 6. They provide the necessary skewness in both the velocity derivative and velocity increments distribution, as will be shown in Sec. VI.

We begin by dividing the unit interval into $2^{\alpha_{\min}}$ pieces, and use p-model construction to generate an intermittent measure in each of these pieces. The number of steps used in the construction is $n-\alpha_{\min}$ because the p-model measure needs to be defined at the finest resolution (2^n points on the unit interval) in order to facilitate complete choice in the selection of random scales and locations for the tent functions, as we shall see later. However, as the size of the smallest tent is $2^{-\alpha_{\max}}$, the effective number of steps in the energy cascade is equal to $\alpha_{\max}-\alpha_{\min}$. This number is fixed by the Reynolds number of the synthetic turbulence signal being generated. We denote by d_β the value of the measure at the smallest interval located at β. The total measure over the interval $[\beta,\beta+2^{-\alpha}]$ will be denoted by D_β, that is, $D_\beta=\sum_{i=\beta}^{\beta+2^{-\alpha}} d_i$. We use the notation d instead of ϵ to emphasize that the measure generated here is not the actual dissipation but an auxiliary dissipationlike quantity.

As remarked earlier, *the synthetic velocity field is a superposition of skewed tent functions of different sizes and amplitudes.* Hence, we need to determine the scale, location, and amplitude of each of these tents in order to define the synthetic turbulence model completely. This is done as follows.

The sizes of the tents $r=2^{-\alpha}$ are chosen randomly from the following distribution:

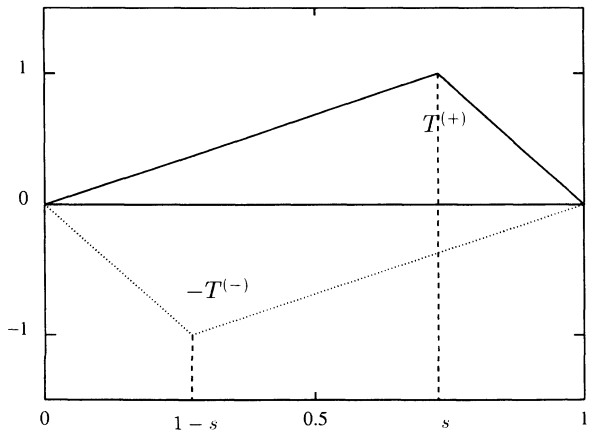

FIG. 6. Basic tent functions $T^{(+)}$ and $T^{(-)}$ used in the synthetic turbulence models. As $T^{(-)}$ will always appear in the construction multiplied by a negative number, we have plotted $-T^{(-)}$.

$$P(\alpha)=\frac{\ln(2)2^{\alpha}}{2^{\alpha_{\max}}-2^{\alpha_{\min}}}, \quad \alpha_{\min}<\alpha<\alpha_{\max}, \tag{11}$$

where $\alpha_{\min}$ and $\alpha_{\max}$ specify the largest and the smallest tents, respectively. This distribution is analogous to the hierarchy of scales present in a cascade process. A given tent of scale r will be localized in the interval $[\beta,\beta+r]$ where the parameter β (which determines the location of the tent) is chosen from the uniform distribution on unit interval. The continuous distribution of scales as well as their random location on the interval satisfy continuous scale and translation symmetries required by Navier-Stokes equations. It is important to note that because of the continuity of the parameter β, the superposition of different tents will produce a viscous crossover scale which fluctuates spatially.

Finally, the amplitude of the tent is a measure of the velocity increment across an interval of size r, which will be determined in the spirit of Kolmogorov's refined similarity hypothesis as the product of a stochastic variable V and $(D_\beta)^{1/3}$. We use a Gaussian distribution with zero mean for the stochastic variable V. The amplitude of the tent will be equal to $U_0 V(\sum_{i=\beta}^{\beta+2^{-\alpha}} d_i)^{1/3}=U_0 V D_\beta^{1/3}$. For random values of β and $r=2^{\alpha}$ chosen from the distributions specified above, we need to know the value of d_i at the finest resolution in order to compute the quantity $\sum_{i=\beta}^{\beta+2^{-\alpha}} d_i$. This necessitates $n-\alpha_{\min}$ steps in the p-model construction as mentioned before. The quantity U_0 provides the velocity units for the amplitude of the tent; it will always appear in conjunction with V. Without loss of generality, we can take $\langle V^2\rangle=1$, and keep U_0 as a parameter. It will be shown later that U_0 corresponds to the root-mean-square (rms) velocity.

In order to preserve the space reversal symmetry of the Navier-Stokes equations, a further consideration is necessary. When the sign of the amplitude (given by the sign of the stochastic variable V) is positive, the tents will be of the form shown in Fig. 6(a) and will be denoted by $T^{(+)}$. When the amplitude is negative (i.e., negative V), the tents will be of the form shown in Fig. 6(b) and denoted by $T^{(-)}$. The expression for $T^{(V)}$ [the superscript (V) indicates the dependence of T on the sign of V] is

$$T^{(+)}(\mu)=\begin{cases}\mu/s & \text{if } 0<\mu<s\\ (1-\mu)/(1-s) & \text{if } s<\mu<1\\ 0 & \text{otherwise}\end{cases} \tag{12}$$

and

$$T^{(-)}(\mu)=\begin{cases}\mu/(1-s) & \text{if } 0<\mu<1-s\\ (1-\mu)/s & \text{if } 1-s<\mu<1\\ 0 & \text{otherwise}.\end{cases} \tag{13}$$

Here s is the skew parameter, as before. In Sec. VI, it will be shown that in order for the synthetic turbulence signal to be consistent with Kolmogorov's $\frac{4}{5}$th law for the third-order structure function [3], $s=0.88$. These tents $T^{(+)}$ and $T^{(-)}$ supported in the interval [0,1] are scaled and positioned with $\mu=2^{\alpha}(x-\beta)$. A certain number N of these tents are superposed to generate the artificial ve-

locity field; the precise value of N will be discussed in Sec. VI. Periodic boundary conditions are assumed for computational convenience. To summarize, the composite model for the velocity is given by

$$u(x)=U_0\sum_{j=1}^{N}\left[V_j\left[\sum_{i=\beta_j}^{\beta_j+2^{-\alpha_j}} d_i\right]^{1/3}\right]T^{(V_j)}(2^{\alpha_j}(x-\beta_j))\ . \tag{14}$$

This expression for $u(x)$ has an alternative interpretation as terms of a wavelet expansion whose coefficients are related to the velocity increments at different scales. However, both α_j and β_j are taken from a continuous distribution unlike a dyadic hierarchy of elements in a wavelet expansion. The distribution of scales [Eq. (11)] constitutes a generalization to the continuous case of a wavelet-basis description of the signal.

B. Skewed tents with underlying l model

As remarked earlier, a synthetic turbulence field can be built up using a binary cascade if we employ an l model for constructing the intermittent measure similar to turbulent energy dissipation. The presence of a wide range of scales in the l-model construction ensures the condition of continuous scale and translational symmetries without the need for parameters α and β. By using skewed tent functions to represent velocity increments, whose shape depends on the sign of the increment itself, one can also satisfy the space reversal symmetry of Navier-Stokes equations. An artificial velocity field so constructed exhibits all the desired statistical properties of skewness and intermittency effects on scaling exponents. A brief description of this method of generating synthetic turbulence is given below. As before, we begin by considering a unit interval on which a measure (analogous to energy dissipation) is assigned a value unity. The unit interval is then divided into two unequal pieces using the l-model multipliers ($l_1=0.7$, $l_2=0.3$), and the measure (which is representative of the quantity $r\epsilon_r$ in turbulence) contained in each piece is equal to $\frac{1}{2}$ of the original measure. Using Kolmogorov's refined similarity hypothesis, the measure contained in each of the pieces is converted into an appropriate velocity increment. The stochastic variable V is chosen from a Gaussian distribution with zero mean and unit variance. These velocity increments represent the amplitude of the skewed tent function described by Eqs. (12) and (13). It was found by numerical trials that the skew parameter s had to be 0.67 in order to obtain the needed skewness. The tents are scaled and located to have the size and position of each of the pieces in the l-model construction. The artificial velocity field is then a simple superposition of all tent functions formed at successive stages of the construction. The number of steps in the construction can be varied according to the Reynolds numbers.

VI. SOME EXACT RESULTS

In order to compare the synthetic turbulence signal with the real turbulence, one has to be able to identify the parameters in the construction of the former with the physical quantities related to the latter. For this purpose, it is helpful to obtain some exact analytical results. While the l model requires less input, it does not unfortunately lend itself to explicit analytical results. On the other hand, the signal generated on the basis of the p model allows a fairly complete theoretical analysis. This is the topic of this section. The parameters of the model are $\alpha_{\min}$, $\alpha_{\max}$, N, U_0, p [see Eq. (6)], and s. However, the parameter N appears only in the combination $\gamma=N/(2^{\alpha_{\max}}-2^{\alpha_{\min}})$, so the relevant list of parameters can be rewritten $\alpha_{\min}$, $\alpha_{\max}$, γ, U_0, p, and s. The physical quantities governing real turbulence are the integral scale L, the root mean square of velocity fluctuations $u_{\rm rms}$, the kinematic viscosity ν, along with some properties inherent to the turbulent state such as the skewness of the velocity increments

$$\langle \Delta u_r^3\rangle/r=-\tfrac{4}{5}\langle\epsilon\rangle\ , \tag{15}$$

where $\Delta u_r\equiv\Delta u(r)$ and the universal scaling exponents of the velocity increments in the inertial range, ζ_n, are given by

$$\langle \Delta u_r^n\rangle\sim\left[\frac{r}{L}\right]^{\zeta_n}\ . \tag{16}$$

In this section we show that a relation can be established between $\alpha_{\min}$ and L, U_0 and $u_{\rm rms}$, $\alpha_{\max}$, and ν, s and the skewness of velocity increments, p and the scaling exponent ζ_n for some single n, say $n=2$. The parameter γ can also be chosen in a sensible way, as we shall see below. After demonstrating this match, some predictions will be derived for the skewness of the derivative. The detailed calculations are rather lengthy and a brief account is given in the Appendix. Consider the second-order moment of the velocity increments, $\langle \Delta u_r^2\rangle$. It is usually written for the range $\eta\ll r\ll L$ as

$$\langle \Delta u_r^2\rangle=C(L\langle\epsilon\rangle)^{2/3}\left[\frac{r}{L}\right]^{\zeta_2}\ , \tag{17}$$

while for synthetic turbulence we find [from Eq. (A14) of the Appendix] that

$$\langle \Delta u_r^2\rangle=\gamma U_0^2 h(s)\left[\frac{r}{2^{-\alpha_{\min}}}\right]^{-\log_2\langle M^{2/3}\rangle} \tag{18}$$

is valid for $2^{-\alpha_{\max}}\ll r\ll(1-s)2^{-\alpha_{\min}}$. A comparison between Eqs. (17) and (18) shows that $-\log_2\langle M^{2/3}\rangle=\zeta_2$. This is verified because the parameters of the p model were chosen such that the experimental value of $\zeta_2=0.7$ yields $p\sim 0.7$ in the equation for distribution of M [Eq. (6)]. It is further seen that $2^{-\alpha_{\min}}$, the size of the largest tent, plays the role of integral scale L. This is consistent with the fact that the velocity autocorrelation vanishes at $2^{-\alpha_{\min}}$ in synthetic turbulence just as it happens at separation distances of the order of L in real turbulence. Measuring lengths in units of the total interval where the construction takes place, allows us to write $L=2^{-\alpha_{\min}}$, and the total interval contains $2^{\alpha_{\min}}$ integral scales. This

gives us the rule to choose $\alpha_{\min}$ when we want to mimic a real turbulence signal: If we want to have a number K of integral scales represented in the construction then $K=2^{\alpha_{\min}}$.

Consider now the variance of the velocity fluctuations. In real turbulence we have $\langle u^2\rangle = u_{\rm rms}^2$. In synthetic turbulence (see Appendix).

$$\langle u^2\rangle = \frac{\gamma}{3\zeta_2}\left[1-\left[\frac{2^{-\alpha_{\min}}}{2^{-\alpha_{\max}}}\right]^{\zeta_2}\right]U_0^2 \ . \tag{19}$$

For $2^{-\alpha_{\min}} \ll 2^{-\alpha_{\max}}$, we obtain

$$\langle u^2\rangle = \frac{\gamma}{3\zeta_2}U_0^2 \ . \tag{20}$$

In order for U_0^2 to represent $u_{\rm rms}^2$ (which is a desirable interpretation), we take $\gamma = 3\zeta_2 \sim 2$. The choice $\gamma=2$ has another justification. If the tents are taken as the basis in a dyadic waveletlike expansion from a minimum scale $2^{-\alpha_{\min}}$ to a maximum scale $2^{-\alpha_{\max}}$ over the unit interval, then the number of tents used in the expansion would be $N = 2^{\alpha_{\max}} + 2^{(\alpha_{\max}-1)} + \cdots + 2^{\alpha_{\min}} = 2^{\alpha_{\max}+1} - 2^{\alpha_{\min}}$. For $2^{\alpha_{\max}} \gg 2^{\alpha_{\min}}$, $\gamma \sim N/2^{\alpha_{\max}} = 2$. Thus we have

$$U_0 \simeq u_{\rm rms} \ . \tag{21}$$

We now compute the value of s that provides the necessary skewness. In homogeneous and isotropic turbulence, the third-order moment of velocity increments in the inertial range is given by

$$\langle \Delta u_r^3\rangle = -\tfrac{4}{5}(\langle\epsilon\rangle L)\frac{r}{L} \ . \tag{22}$$

For the synthetic turbulence model, this same quantity can be shown to be [see Appendix, Eq. (A15)]

$$\langle \Delta u_r^3\rangle = \frac{4\gamma}{\sqrt{2\pi}}U_0^3 g(s)\frac{r}{2^{-\alpha_{\min}}} \tag{23}$$

in the interval $2^{-\alpha_{\min}} \ll r < 2^{-\alpha_{\max}}$, where $g(s)$ is defined in the Appendix. Using $2^{-\alpha_{\min}} = L$ and $\gamma = 2$ and matching the prefactors in Eqs. (22) and (23), we obtain

$$g(s) = \frac{\sqrt{2\pi}}{10}\frac{\langle\epsilon\rangle L}{U_0^3} \ . \tag{24}$$

In turbulent flows the quantity $L\langle\epsilon\rangle/u_{\rm rms}^3 \equiv A$ is of the order of unity [16] but is not a universal quantity. The quantity can be explicitly computed for the synthetic turbulence model. To do so, we equate the prefactors to r/L in Eqs. (17) and (18) to find that

$$[h(s)]^{3/2} = \left[\frac{C}{2}\right]^{2/3}\frac{\langle\epsilon\rangle L}{U_0^3} \ . \tag{25}$$

Taking the value $C=2$ (approximately correct from experimental measurements) we find from Eqs. (24) and (25) that s is given by

$$\frac{h(s)^{3/2}}{g(s)} = \frac{10}{\sqrt{2\pi}} \ . \tag{26}$$

We solved the above equation numerically and found that $s=0.88$. Substituting this value in Eq. (24), we find that

$$\frac{\langle\epsilon\rangle L}{U_0^3} = 4.27 \tag{27}$$

for the synthetic turbulence model. As already remarked, for real turbulence the ratio $(\langle\epsilon\rangle L)/u_{\rm rms}^3 \equiv A$ is close to unity for high enough values of the Reynolds number. Hence the dissipation average for synthetic turbulence will not in general be the same as that of real turbulence. Denoting $\langle\epsilon\rangle_{\rm ST}$ as the average dissipation for the synthetic turbulence, we have $\langle\epsilon\rangle_{\rm ST} = (4.27/A)\langle\epsilon\rangle$.

In order to relate $\alpha_{\max}$ to a suitable turbulence parameter, let us first define a quantity η^* as the scale at which the equality

$$\left\langle\left[\frac{\Delta u(\eta^*)}{\eta^*}\right]^2\right\rangle = \left\langle\left[\frac{\partial u}{\partial x}\right]^2\right\rangle \tag{28}$$

holds, where the left side of Eq. (28) is computed using Eq. (17) (i.e., as an inertial range quantity) and the right-hand side of Eq. (28) is clearly a dissipation range quantity. The scale η^*, therefore, can be interpreted as the upper bound of the dissipative range or the lower bound of the inertial range. Recalling from theory of isotropic turbulence [21] that

$$\left\langle\left[\frac{\partial u}{\partial x}\right]^2\right\rangle = \frac{\langle\epsilon\rangle}{15\nu} \ , \tag{29}$$

we find that

$$\frac{Lu_{\rm rms}}{\nu} = \frac{15C}{A^{1/3}}\left[\frac{\eta^*}{L}\right]^{\zeta_2-2} \ . \tag{30}$$

(Notice that the left-hand side of the above equation is the Reynolds number.) Approximating $\zeta_2 \sim \frac{2}{3}$, and taking $C=2$ and $A=1$, we find that $\eta^* = (30)^{3/4}\eta \sim 13\eta$, where $\eta = (\nu^3/\langle\epsilon\rangle)^{1/4}$ is the Kolmogorov scale. Returning to the case of synthetic turbulence it follows from Eq. (A8) in the Appendix that for $2^{-\alpha_{\max}} \ll 2^{-\alpha_{\min}}$,

$$\left\langle\left[\frac{\partial u}{\partial x}\right]^2\right\rangle = \frac{U_0^2}{L^2}\frac{2}{s(1-s)(2-\zeta_2)}\left[\frac{L}{2^{-\alpha_{\max}}}\right]^{2-\zeta_2} \ . \tag{31}$$

As is the case in real turbulence, we wish that

$$\left\langle\left[\frac{\partial u}{\partial x}\right]^2\right\rangle = \frac{\langle\epsilon\rangle_{\rm ST}}{15\nu} \ , \tag{32}$$

where we take the synthetic turbulence kinematic viscosity equal to the kinematic viscosity of the fluid whose turbulent flow we are trying to mimic. On inserting Eqs. (32) and (27) in Eq. (31), we obtain the equivalent of Eq. (30) for synthetic turbulence, namely,

$$\frac{LU_0}{\nu} = 51.3\left[\frac{L}{2^{-\alpha_{\max}}}\right]^{2-\zeta_2} \ . \tag{33}$$

Equation (33) can readily be used to compute $\alpha_{\max}$. Its similitude with Eq. (30) also provides a clear interpretation of $2^{-\alpha_{\max}}$: it plays the same role as η^* in real tur-

bulence. It is easy to show that

$$2^{-\alpha_{\max}}/2^{-\alpha_{\min}}=1.5(\eta^*/L)\ . \tag{34}$$

All the parameters in the model have now been related to some measurable quantity in a turbulent signal. It should be stressed that this matching between the model and real turbulence is not unique. The matching attempted here is, however, dictated by the physical interpretation of each of the parameters in the model. We now compute the derivative skewness defined as

$$S=\frac{\left\langle\left[\frac{\partial u}{\partial x}\right]^3\right\rangle}{\left\langle\left[\frac{\partial u}{\partial x}\right]^2\right\rangle^{3/2}}\ . \tag{35}$$

From Eq. (A6) in the Appendix, we obtain

$$\left\langle\left[\frac{\partial u}{\partial x}\right]^3\right\rangle=\frac{U_0^3}{L^3}\frac{4}{\sqrt{2\pi}}\frac{1-2s}{s^2(1-s)^2}\left[\frac{2^{2\alpha_{\max}}}{2^{2\alpha_{\min}}}-1\right]\ . \tag{36}$$

From Eqs. (A7) and (36), given the inequality that $2^{\alpha_{\max}}\gg 2^{\alpha_{\min}}$, we obtain

$$S=\frac{(2-\zeta_2)^{3/2}}{\sqrt{\pi}}\frac{1-2s}{\sqrt{s(1-s)}}\left[\frac{2^{\alpha_{\max}}}{2^{\alpha_{\min}}}\right]^{(3\zeta_2-2)/2}\ . \tag{37}$$

In these equations it is clear that the skewness would be zero if s were $1/2$. Using the fact that $2^{\alpha_{\max}}/2^{\alpha_{\min}}\propto L/\eta^*\sim \mathrm{Re}^{1/(2-\zeta_2)}$ (where $\mathrm{Re}=LU_0/\nu$), we are led to conclude that

$$S\sim \mathrm{Re}^{(3\zeta_2-2)/(4-2\zeta_2)}\ . \tag{38}$$

It is interesting to note that in the context of Kolmogorov's 1941 theory, Eq. (38) predicts a skewness coefficient independent of the Reynolds number; however, with intermittency corrections, this model predicts that the skewness varies as some small power of the Reynolds number, as appears to be true experimentally [22]. Before concluding this section, we should remark on a related technique to generate a velocity field. Let the dissipation contained in an interval of size $2^{-\alpha}$ be given by $\prod_{i=1}^{\alpha}m_i$ [where m_i's are a set of random multipliers picked from a given distribution, e.g., Eq. (6)] irrespective of the location of the interval (that is, without using a hierarchical p-model construction). If this value of dissipation is converted into an appropriate velocity increment, and these velocity increments are combined in a manner similar to the synthetic turbulence technique, the resulting artificial velocity signal suffers from a curious drawback. It can be analytically shown that structure functions of order *four* and higher exhibit mixed scaling (e.g., $\langle\Delta u_r^4\rangle\sim Ar^{\zeta_4}+Br^{2\zeta_2}$ where A and B are constants and can be easily computed). It can be shown analytically that this does not occur for the synthetic turbulence model described in Sec. V A. This observation emphasizes the need for correlated multipliers for generating an intermittent measure analogous to dissipation for obtaining correct scaling for structure functions of all orders.

VII. COMPARISONS WITH EXPERIMENTAL DATA

We shall now compare the artificial stochastic field generated using both the synthetic turbulence models (continuous p model as well as the l model) with experimental time series of velocity fluctuations obtained in the atmospheric boundary layer. Note that the time series data will be interpreted as a spatial cut through the turbulent velocity field in the direction of the mean flow. This so-called Taylor's hypothesis has been extensively used in the turbulence literature in spite of its inadequacies which have been pointed out repeatedly. The experimental data were acquired using a hot-wire probe 2 m above the roof of a four-story building. We believe that these measurements are sufficiently far away from solid boundaries that they are not *directly* affected by the presence of the boundary—even though, of course, the boundary is eventually responsible for the generation of turbulence. The integral scale of the flow was of the order of the height of the measuring station above ground level ($\sim$18 m). The Reynolds number of the flow based on the integral scale was 7×10^6. The Taylor microscale was computed to be 5.3 cm, whereas the Kolmogorov microscale was 0.07 cm. The sampling frequency was 6000 Hz and the number of data points acquired was 127 000. Also the mean velocity of the flow at hot-wire location was 6 m/s and the root-mean-square velocity fluctuation was 42 cm/s. Using the relations between parameters of real turbulence and synthetic turbulence discussed in the previous section, it was determined from the parameter matching of Sec. VI that a model signal with 2^{17} data points and $\alpha_{\min}=5$ and $\alpha_{\max}=14$ would be suitable for the purpose of comparisons with experimental data.

In Fig. 7 we show an example of a spatial section from the two synthetic turbulence models with above parameters along with a representative experimental turbulent time series. The model signals are qualitatively similar to real turbulence signals. The real turbulent signal spans approximately two integral scales. Figure 8 shows a plot of the power spectrum of the synthetic turbulence signals for the two cases. The three salient features that can be observed in this figure are

(a) In the inertial range [intermediate wave numbers corresponding to scales between $2^{-\alpha_{\max}}$ and $(1-s)2^{-\alpha_{\min}}$], the spectrum exhibits a power-law behavior $\sim k^{-\beta}$. The power spectral exponent β determined from the figure is 1.71, which is in close agreement with real turbulence.

(b) The dissipative range behavior (large wave numbers corresponding to scales smaller than $2^{-\alpha_{\max}}$): Given that the (statistically) self-similar construction ends at scales $2^{-\alpha_{\max}}$, it is expected that $k^{-\beta}$ scaling will no longer hold for smaller scales. Actually, as the functions used in the construction are smooth (essentially linear) at this resolution, we expect a relatively steep decay in the spectrum. While this is qualitatively similar to the situation in turbulence, the results at these scales will depend on the form of tent functions and so we should not expect quantitative correspondence to real turbulence.

(c) The large-scale behavior (small wave numbers cor-

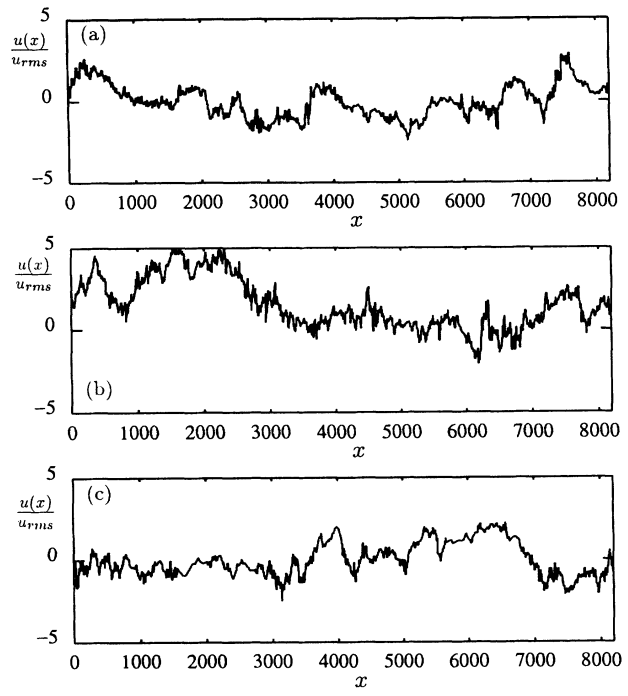

FIG. 7. Examples of velocity sections from (a) atmospheric turbulence, (b) synthetic turbulence based on the p model, (c) synthetic turbulence based on the l model. The data cover approximately two integral scales.

responding to scales larger than $2^{-\alpha_{\min}}$): It is not readily apparent that a model which emphasizes a self-similar construction containing inertial-range physics should exhibit integral scale features. However, in the construction for $r > L$, the velocity $u(x)$ at location x is composed of tents that are independent of the ones composing the signal at location $x+r$. Therefore, the correlation of velocity vanishes at scales beyond $2^{-\alpha_{\min}}$, leading to a flat region in the spectrum at large scales.

Another quantity of interest in characterizing the statistical features of turbulent fluctuations is the velocity structure function, $\langle \Delta u_r^n \rangle = \langle [u(x+r)-u(x)]^n \rangle \sim r^{\zeta_n}$, where n is the order of the structure function and ζ_n is the corresponding structure function exponent. Figure 9(a) shows a comparison for the second-order structure function between the one obtained experimentally and that corresponding to synthetic turbulence signals. As with the power spectrum, the three regions corresponding to dissipative scales ($\langle \Delta u_r^2 \rangle \sim r^2$), inertial-range scales ($\langle \Delta u_r^2 \rangle \sim r^{\zeta_2}$), and the large scales ($\langle \Delta u_r^2 \rangle \sim$ const), can be clearly identified. Similarly, Fig. 9(b) shows the comparison for the third-order structure function. The experimental scatter in Fig. 9(b) at large values of r/L is due to the poor convergence caused by insufficient data. (In general the odd-order structure functions take longer to converge.) Even so, the models capture these two essential properties of turbulent signals. The scaling exponents ζ_n as a function of n are shown in Fig. 10. They were obtained by averaging over 64 realizations of the model signals to ensure statistical convergence. The deviations from $\zeta_n = n/3$ indicate the effects of small-scale intermittency. The ζ_n for real turbulence data are taken from Ref. [23].

The fractal dimension of the synthetic turbulence signals was computed using the ϵ- *variation* method suggest-

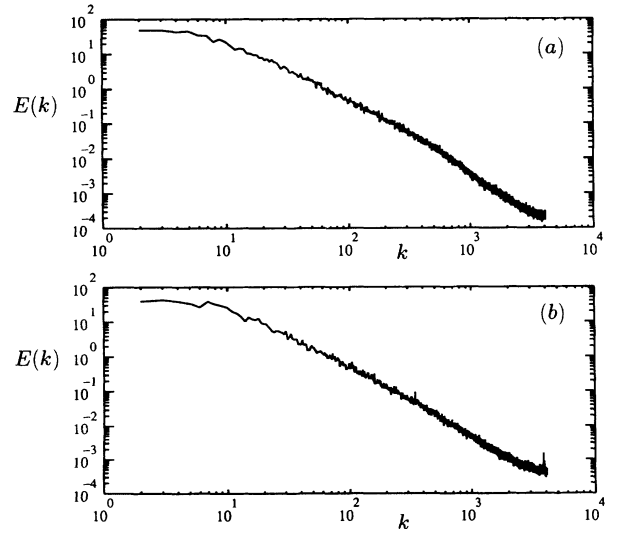

FIG. 8. The spectral density of the synthetic velocity field obtained on the basis of (a) the p model and (b) the l model. Four realizations with $\alpha_{\min}=5$ and $\alpha_{\max}=14$ were averaged. Note that, in (a), $k_{\eta^*}=2\pi/\eta^* \approx 4000$, and $k_{L^*}=2\pi L \approx 5$.

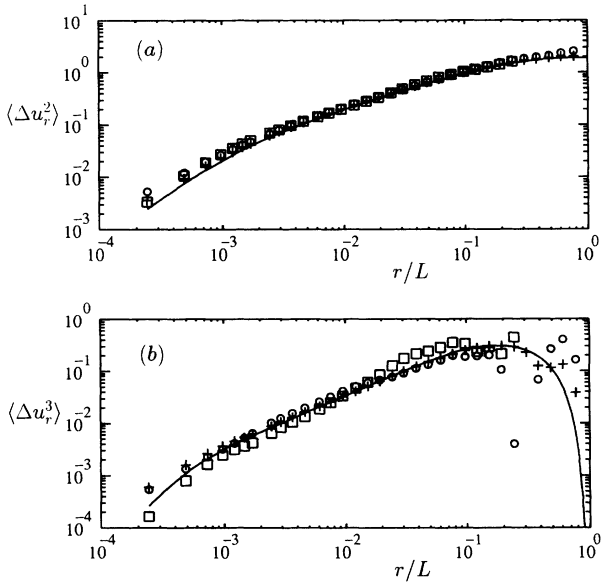

FIG. 9. Comparison of (a) *the second-order structure function* and (b) *the third-order structure function* obtained from velocity data in atmospheric turbulence and synthetic turbulence. □ denotes experimental data, + denotes synthetic turbulence based on the p model, and ○ denotes synthetic turbulence based on the l model. The solid lines represent the theoretical predictions for synthetic turbulence based on the p model [Eqs. (18) and (23) in the text].

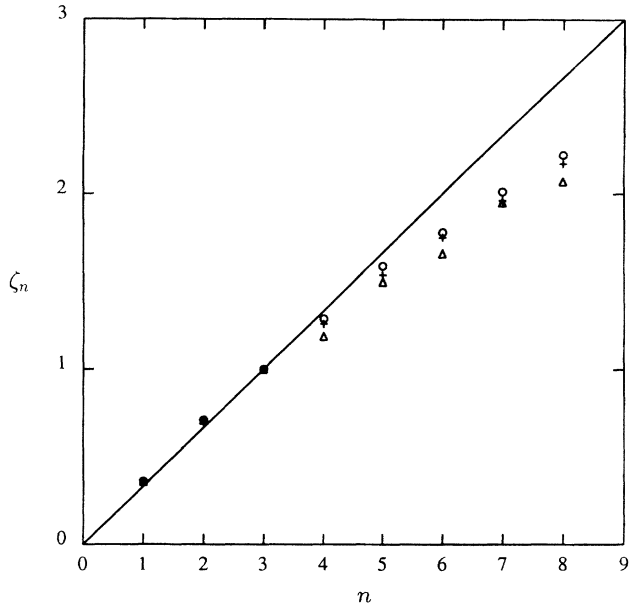

FIG. 10. Comparison of structure function exponents obtained from experimental turbulence data (○), synthetic turbulence based on the p model (△), and synthetic turbulence based on the l model (+). Solid line denotes Kolmogorov's 1941 theory (K41), $\zeta_n = n/3$.

ed by Dubuc *et al.* [24], which gives robust results in case of self-affine curves. The fractal dimension can be inferred from the slope of the plot between $(\log_{10}(1/r), \log_{10}[1/r^2 B(r,f)])$, where $B(r,f)$ is the variation of the self-affine function f in the r neighborhood. For details see Ref. [24]. Figure 11 shows the relevant plots for the synthetic turbulence signals implying the fractal dimension in both the cases is approximately 1.67, in very good agreement with experimental measurements ($D = 1.65 \pm 0.05$ as shown in Ref. [1]).

Figure 12 shows a section of the energy dissipation field obtained from the real turbulent velocity fluctuations as well as the synthetic turbulence signals. It is readily apparent that they exhibit similar features of small-scale intermittency. This can also be quantified by computing the intermittency exponent μ for the dissipation from the synthetic turbulence signals. One way of determining μ is from the slope of a plot of $\log_{10}\langle (r\epsilon_r)^2 \rangle$ *versus* $\log_{10} r$ [shown in Figs. 13(a) and 13(b)] for the synthetic turbulence signals generated using p-model construction and l-model construction, respectively]. Using the relation $\langle \epsilon_r^2 \rangle \sim r^{-\mu}$ together with the slopes computed in Fig. 13, it was found that $\mu = 0.24$ in the first case and $\mu = 0.28$ in the second case, which is in good agreement with the results in real turbulence ($\mu = 0.25 \pm 0.05$ from [25]) and also consistent with multifractal formalism of energy dissipation [12].

We now verify whether Kolmogorov's refined similarity hypotheses hold true in the case of synthetic turbulence as well. The conditional probability distribution function (PDF) of the stochastic variable $V_{\mathrm{RSH}} = \Delta u(r)/(r\epsilon_r)^{1/3}$ [see Eq. (7)] is computed for some $r\epsilon_r$ values and for two values of r/L, one in the dissipative range and the other in the inertial range; the results are shown in Fig. 14. Figures 14(a) and 14(b) are for experimental turbulence while Figs. 14(c) and 14(d) are for synthetic turbulence generated using the p-model construc-

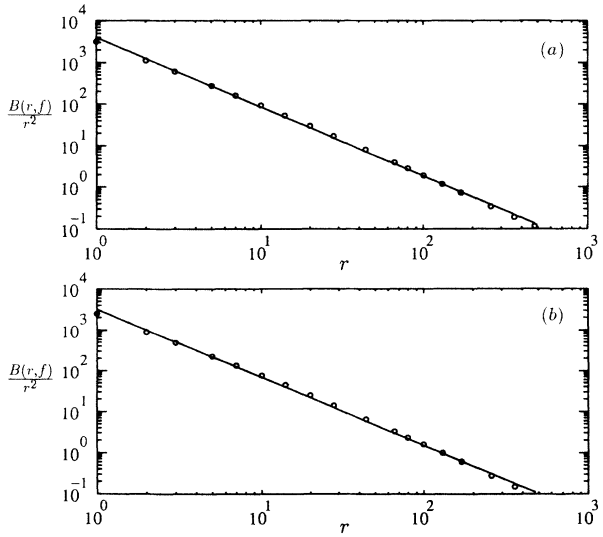

FIG. 11. Estimation of fractal dimension for artificial velocity signals from (a) synthetic turbulence based on the p model (slope of the best linear fit is -1.665), (b) synthetic turbulence based on the l model (slope of the best linear fit is -1.667).

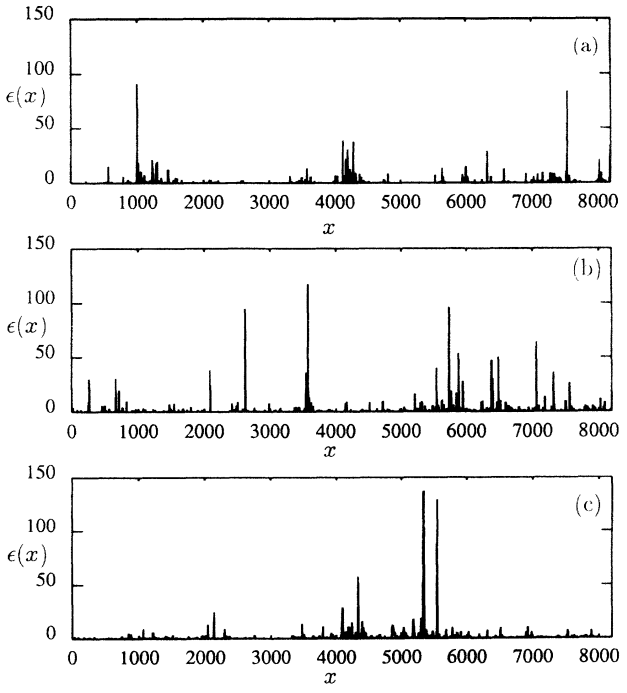

FIG. 12. Examples of dissipation fields constructed from velocity signals for (a) atmospheric turbulence, (b) synthetic turbulence based on the p model, (c) synthetic turbulence based on the l model.

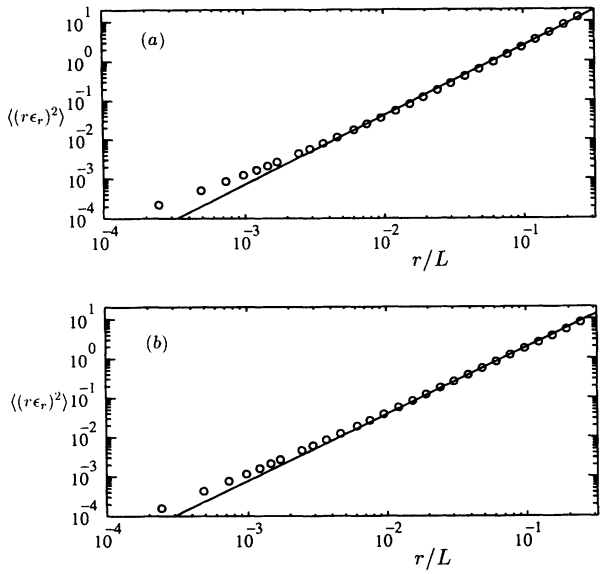

FIG. 13. Scaling of $\langle(r\epsilon_r)^2\rangle$ for the dissipation field constructed from (a) synthetic turbulence based on the p model (slope of the best linear fit is 1.76) (b) synthetic turbulence based on the l model (slope of the best linear fit is 1.72).

tion, and Figs. 14(e) and 14(f) are for synthetic turbulence based on the l model. The synthetic turbulence does not duplicate the small-scale (dissipative range) features of real turbulence very well, although the l model seems to be quite close. However, for inertial-range scales, the synthetic turbulence signal reproduces the PDF's obtained in real turbulence, even though the l-model construction yields a somewhat poorer collapse of the conditional PDF's of V_{RSH} in the inertial range. For the synthetic turbulence based on the p model, these PDF's appear to be independent of $r\epsilon_r$ as postulated by Kolmogorov. This conclusion holds true for different values of r in the inertial range (not shown here).

VIII. CONCLUSIONS

Two simple schemes have been presented for generating a turbulencelike stochastic field (synthetic turbulence) and are implemented in one dimension. The schemes are based either on the p model and the l model for the energy dissipation. The implementation is quite straightforward and needs little by way of computer requirements, and can be related to any desired flow Reynolds number.

The properties of the synthetic turbulence signals have been compared with those of real turbulence. The comparisons include power spectral density, odd and even order structure functions, fractal dimension, skewness of velocity increments, PDF of universal stochastic variable V_{RSH}, and the multifractal scaling of the dissipation field. In all these respects, the two schemes yield signals which are very close to each other and to real turbulent velocity. The only difference between the two schemes concerns the property of V_{RSH}, but these differences are not fundamental. The success of the schemes suggests that the physical elements that go into their construction are good abstractions of the reality, and further that the statistical ordering in turbulence can be approximated relatively simply for most practical purposes.

The schemes presented in this paper are aimed at representing one-dimensional cuts of three-dimensional velocity fields. The extension of these schemes to represent the full three-dimensional velocity field is relatively easy and is in progress. That one can cheaply generate stochastic fields that are so close to turbulence, away from the boundaries at any Reynolds number, suggests that a practical utility of the present schemes (actually, their extensions to three dimensions) is that they can provide realistic initial conditions for direct numerical simulations of the Navier-Stokes equations. The boundary effects can also be included, but this is a matter of future research.

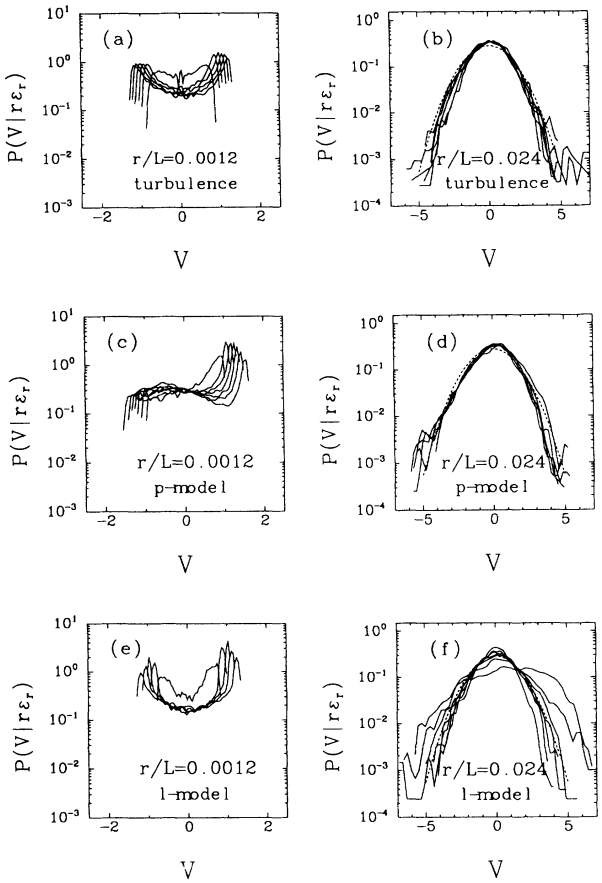

FIG. 14. Conditional PDF's of $V_{\mathrm{RSH}}=\Delta u_r/(r\epsilon_r)^{1/3}$, given $r\epsilon_r$, for two values of $/L$ (indicated in the figure) for atmospheric boundary layer [(a) and (b)], synthetic turbulence based on p model [(c) and (d)], and synthetic turbulence based on the l model [(e) and (f)]. In each plot, the several curves correspond to different values of $r\epsilon_r/L\langle\epsilon\rangle$ ranging between 4.9×10^{-5} and 1.0×10^{-3} in (a), 1.6×10^{-3} and 3.1×10^{-2} in (b), 3.6×10^{-5} and 1.2×10^{-3} in (c), 3.7×10^{-3} and 4.4×10^{-2} in (d), 1.2×10^{-5} and 4.9×10^{-4} in (e), and 1.2×10^{-3} and 5.8×10^{-2} in (f). The dashed curves in (b), (d), and (f) represent Gaussian PDF's with the variance equal to 2.

ACKNOWLEDGMENTS

We thank Professor Peter Jones for some perspicuous comments in the early stages of the work, and Professor S. Grossmann for many useful comments on an earlier draft. The work was supported by AFOSR and DARPA.

APPENDIX

In this Appendix we derive some of the expressions used in the text, and explicitly compute some of the quantities of interest. We will denote with $\langle\ \rangle_z$, the expectation with respect to the distribution of z. Periodic boundary conditions are assumed.

(a) Computation of $\langle u^2\rangle$. The calculations proceed by computing averages over the random variables used in the synthetic turbulence signal, namely, V, β, α, and the multipliers M. On using Eq. (14) we have that

$$\langle u^2\rangle = U_0^2 \sum_{j_1=1}^{N}\sum_{j_2=1}^{N} \langle \langle D_{j_1}^{1/3} D_{j_2}^{1/3}\rangle_M \times \langle V_{j_1} V_{j_2} T^{(V_{j_1})}(\mu_{j_1}) \times T^{(V_{j_2})}(\mu_{j_2})\rangle_V \rangle_{\beta,\alpha}\ , \tag{A1}$$

where $D_j = \sum_{i=\beta_j}^{\beta_j+2^{-\alpha_j}} d_i$, and $\mu_j = 2^{\alpha_j}(x-\beta_j)$. The sums D_j can be well approximated by $D_j \approx \prod_{n=1}^{\alpha_j-\alpha_{\min}} M_n$, where the M_n are the multipliers used to construct the dissipation field. Then, the M average of the dissipation term raised to the power q is

$$\langle D_j^q\rangle_M = \left\langle \left[\sum_{i=\beta_j}^{\beta_j+2^{-\alpha_j}} \epsilon_i \right]^q \right\rangle_M \approx \left\langle \left[\prod_{n=1}^{\alpha_j-\alpha_{\min}} M_n \right]^q \right\rangle = \left[\frac{2^{-\alpha_j}}{2^{-\alpha_{\min}}} \right]^{\zeta_{3q}}\ , \tag{A2}$$

where $\zeta_{3q} = -\log_2\langle M^q\rangle$. Notice that the M averages of D_j^q turn out to be independent of β.

The β average will then only affect the term $\langle V_{j_1} V_{j_2} T^{(V_{j_1})}(\mu_{j_1}) T^{(V_{j_2})}(\mu_{j_2})\rangle_{V,\beta}$ in Eq. (A1). This last term is nonzero only when $j_1 = j_2$. In effect, if $j_1 \neq j_2$, the average over V can be factorized into two identical terms of the form

$$\begin{aligned}\langle V T^{(V)}(\mu)\rangle_{V,\beta} &= \left\langle \int_{-\infty}^{0} dV G(V) V T^{(-)}(\mu) + \int_{0}^{\infty} dV G(V) V T^{(+)}(\mu) \right\rangle_\beta \\ &= \int_0^\infty dV G(V) V [\langle T^{(+)}(\mu)\rangle_\beta - \langle T^{(-)}(\mu)\rangle_\beta] \\ &= 0\ ,\end{aligned} \tag{A3}$$

where $G(V)$ stands for the probability density of V [a Gaussian with zero mean and variance $\langle V^2\rangle$], and we have used $\langle T^{(+)}(\mu)\rangle_\beta = \langle T^{(-)}(\mu)\rangle_\beta$. The terms with $j_1 = j_2$ cannot be factorized, and we find that

$$\begin{aligned}\langle V^2 [T^{(V)}(\mu)]^2\rangle_{V,\beta} &= \int_{-\infty}^{0} dV G(V) V^2 \langle [T^{(-)}(\mu)]^2\rangle_\beta + \int_0^\infty dV G(V) V^2 \langle [T^{(+)}(\mu)]^2\rangle_\beta \\ &= \langle V^2\rangle 2^{-\alpha}/3\ .\end{aligned} \tag{A4}$$

Here, we have used the result $\langle [T^{(-)}(\mu)]^2\rangle = \langle [T^{(+)}(\mu)]^2\rangle = \frac{1}{3}2^{-\alpha}$. The final result is that

$$\begin{aligned}\langle u^2\rangle &= \frac{U_0^2}{2^{-\alpha_{\min}\zeta_2}} \frac{N}{3} \langle 2^{-\alpha(\zeta_2+1)}\rangle_\alpha \\ &= \gamma \frac{U_0^2}{3\zeta_2} \left[1 - \left[\frac{2^{-\alpha_{\max}}}{2^{-\alpha_{\min}}} \right]^{\zeta_2} \right]\ ,\end{aligned} \tag{A5}$$

where we have used the distribution of Eq. (11) to make the α average and $\gamma = N/(2^{-\alpha_{\max}} - 2^{-\alpha_{\min}})$.

(b) Computation of $\langle (\partial u/\partial x)^3\rangle$. Taking the derivative in Eq. (14), and raising the result to the third power, we have

$$\left\langle \left[\frac{\partial u}{\partial x} \right]^3 \right\rangle = U_0^3 \sum_{j_1=1}^{N}\sum_{j_2=1}^{N}\sum_{j_3=1}^{N} \left\langle \langle D_{j_1}^{1/3} D_{j_2}^{1/3} D_{j_3}^{1/3}\rangle_M \left\langle V_{j_1} V_{j_2} V_{j_3} \frac{\partial T^{(V_{j_1})}(\mu_{j_1})}{\partial x} \frac{\partial T^{(V_{j_2})}(\mu_{j_2})}{\partial x} \frac{\partial T^{(V_{j_3})}(\mu_{j_3})}{\partial x} \right\rangle_{V,\beta} \right\rangle_\alpha . \tag{A6}$$

Here, we have used that the fact that M averages of the D_j's are β independent. In performing the average with respect to V and β, three possibilities can occur (i) The three j's are different: In this case the average factorizes into three terms of the form $\langle V\partial T^{(V)}(\mu)/\partial x\rangle_{V,\beta}$. Splitting this average into a positive and a negative part as in (a) above, we obtain that the previous average is equal to $(\int_0^\infty dVVG(V))[\langle\partial T^{(+)}(\mu)/\partial x\rangle_\beta - \langle\partial T^{(-)}(\mu)/\partial x\rangle_\beta]$. This is identically zero because $\langle\partial T^{(-)}(\mu)/\partial x\rangle_\beta=\langle\partial T^{(+)}(\mu)/\partial x\rangle_\beta=0$. (ii) Only two of the three j's are equal. In this case, the average with respect to V and β factorizes into $\langle V^2[\partial T^{(V)}(\mu)/\partial x]^2\rangle_{V,\beta}\langle V\partial T^{(V)}(\mu)/\partial x\rangle_{V,\beta}$ which is equal to zero because the second term vanishes as shown in (i). (iii) The three j's coincide. This is the only case in which the average with respect to V and β yields a nonzero result. Explicitly, $\langle V^3[\partial T(\mu)/\partial x]^3\rangle_{V,\beta}=(\langle|V|^3\rangle/2)\{\langle[\partial T^{(+)}(\mu)/\partial x]^3\rangle_\beta - \langle[\partial T^{(-)}(\mu)/\partial x]^3\rangle_\beta\}$. It is not difficult to see that $\langle|V|^3\rangle=4\langle V^2\rangle^{3/2}/\sqrt{2\pi}$ and that $\langle[\partial T^{(+)}(\mu)/\partial x]^3\rangle_\beta = -\langle[\partial T^{(-)}(\mu)/\partial x]^3\rangle_\beta=2^{2\alpha}(1-2s)/s^2(1-s)^2$. Therefore, Eq. (A6) becomes

$$\left\langle\left[\frac{\partial u}{\partial x}\right]^3\right\rangle=NU_0^3\left\langle\frac{2^{-\alpha}}{2^{-\alpha_{\min}}}\frac{4\langle V^2\rangle^{3/2}}{\sqrt{2\pi}}\frac{2^{2\alpha}(1-2s)}{s^2(1-s)^2}\right\rangle_\alpha .$$

$$=\left[\frac{U_0}{2^{-\alpha_{\min}}}\right]^3\frac{2\langle V^2\rangle^{3/2}}{\sqrt{2\pi}} \times\gamma\frac{(1-2s)}{s^2(1-s)^2}\left[\frac{2^{2\alpha_{\max}}}{2^{2\alpha_{\min}}}-1\right] . \tag{A7}$$

(c) Computation of $\langle(\partial u/\partial x)^2\rangle$. As in (b) above, it can be shown that

$$\left\langle\left[\frac{\partial u}{\partial x}\right]^2\right\rangle=\left[\frac{U_0}{2^{-\alpha_{\min}}}\right]^2\langle V^2\rangle\gamma\frac{2^{(2-\zeta_2)(\alpha_{\max}-\alpha_{\min})}-1}{s(1-s)(2-\zeta_2)} . \tag{A8}$$

(d) Computation of the second-order structure function $\langle\Delta u_r^2\rangle$. From Eq. (14), the second-order structure function can be written as

$$\langle\Delta u_r^2\rangle=\sum_{j_1=1}^N\sum_{j_2=1}^N\langle\langle D_{j_1}^{1/3}D_{j_2}^{1/3}\rangle_m\langle V_{j_1}\Delta T_{j_1}^{(V_{j_1})} \times V_{j_2}\Delta T_{j_2}^{(V_{j_1})}\rangle_{V,\beta}\rangle_\alpha , \tag{A9}$$

where $\Delta T_j^{(V_j)}=T^{(V_j)}(2^{\alpha_j}(x+r-\beta_j))-T^{(V_j)}(2^{\alpha_j}(x-\beta_j))$. If $j_1\neq j_2$, we have

$$\langle V_{j_1}V_{j_2}\Delta T_{j_1}^{(V)_{j_1}}\Delta T_{j_2}^{(V)_{j_1}}\rangle_{V,\beta} =\langle V_{j_1}\Delta T_{j_1}^{(V_{j_1})}\rangle_{V,\beta}\langle V_{j_2}\Delta T_{j_2}^{(V_{j_2})}\rangle_{V,\beta} . \tag{A10}$$

We then compute

$$\langle V\Delta T^{(V)}\rangle_{V,\beta}=\left[\int_0^\infty dVVG(V)\right]\langle\Delta T^{(+)}\rangle_\beta + \left[\int_{-\infty}^0 dVVG(V)\right]\langle\Delta T^{(-)}\rangle_\beta =0 , \tag{A11}$$

because $\langle\Delta T^{(+)}\rangle_\beta=\langle\Delta T^{(-)}\rangle_\beta=0$. Only the case $j_1=j_2$ survives in Eq. (A9). On using that $\langle\Delta T^{(+)2}\rangle_\beta=\langle\Delta T^{(-)2}\rangle_\beta$ in this case, we have $\langle V^2\Delta T^{(V)2}\rangle=\langle V^2\rangle(\Delta T^{(+)})^2=\langle V^2\rangle(\Delta T^{(-)})^2$ and obtain

$$\langle\Delta u_r^2\rangle_{\alpha,\beta,m,V}=U_0^2\sum_{j=1}^N\langle V^2\rangle_V\langle\langle D^{2/3}\rangle_M\langle\Delta T^2(r)\rangle_\beta\rangle_\alpha . \tag{A12}$$

The average of ΔT^2 over $\beta(\langle\Delta T^2\rangle_\beta)$ will be independent of x because the distribution of β is uniform and periodic boundaries are assumed (to avoid x dependencies on boundary effects). As ΔT is piecewise linear, the integrals can be carried out explicitly. After lengthy integration, one obtains

$$\langle\Delta T^2(r)\rangle_\beta=2^{-\alpha}\times\begin{cases}\dfrac{(r2^\alpha)^2}{s(1-s)}-\dfrac{(r2^\alpha)^3}{3}\left\{\dfrac{1+s}{s^2}+\dfrac{2-s}{(1-s)^2}\right\} & \text{if } 0\le r2^\alpha<(1-s)\\ (r2^\alpha)^2\dfrac{1}{s}-\dfrac{(r2^\alpha)^3}{3}\dfrac{1+s}{s^2}-\dfrac{(1-r2^\alpha)^3}{3}\dfrac{1}{s}+\dfrac{1}{3} & \text{if } (1-s)\le r2^\alpha<s\\ \dfrac{2}{3}-\dfrac{(1-r2^\alpha)^3}{3}\left\{\dfrac{1}{s(1-s)}\right\} & \text{if } s\le r2^\alpha<1\\ \frac{2}{3} & \text{if } 1\le r2^\alpha .\end{cases} \tag{A13}$$

Using Eq. (A13) and the result that $\langle D^{2/3}\rangle=(2^{-\alpha}/2^{-\alpha_{\min}})^{\zeta_2}$, we can proceed with the α-average indicated in Eq. (A12). The result can be partitioned into four subregions for r. We quote below the result for r in the inertial range $[2^{-\alpha_{\max}}\le r\le(1-s)2^{-\alpha_{\min}}]$:

$$\frac{\langle\Delta u^2\rangle}{U_0^2\langle V^2\rangle\gamma}=\left[\frac{r}{2^{-\alpha_{\min}}}\right]^2\frac{-1}{s(1-s)(2-\zeta_2)}+\left[\frac{r}{2^{-\alpha_{\min}}}\right]^3\frac{(s-1)^2+s}{s^2(1-s)^2 3(3-\zeta_2)}-\frac{2}{3\zeta_2}\left[\frac{2^{-\alpha_{\max}}}{2^{-\alpha_{\min}}}\right]^{\zeta_2}+\left[\frac{r}{2^{-\alpha_{\min}}}\right]^{\zeta_2}h(s) , \tag{A14}$$

where

$$h(s)=\frac{(1-s)^{2-\zeta_2}}{s(1-s)(2-\zeta_2)}-\frac{(1-s)^{3-\zeta_2}[(s-1)^2+s]}{3s^2(1-s)^2(3-\zeta_2)}-\frac{s^{3-\zeta_2}-(1-s)^{3-\zeta_2}}{2s^2(3-\zeta_2)}$$
$$+\frac{s^{1-\zeta_2}-(1-s)^{1-\zeta_2}}{s(1-\zeta_2)}+\frac{[s^{-\zeta_2}-(1-s)^{-\zeta_2}](1-s)}{3s\zeta_2}+\frac{1-s^{-\zeta_2}}{3s(1-s)\zeta_2}$$
$$-\frac{2(1-s^{-\zeta_2})}{3\zeta_2}+\frac{1-s^{1-\zeta_2}}{s(1-s)(1-\zeta_2)}-\frac{1-s^{2-\zeta_2}}{s(1-s)(2-\zeta_2)}+\frac{1-s^{3-\zeta_2}}{3s(1-s)(3-\zeta_2)}+\frac{2}{3\zeta_2}\ .$$

(e) Computation of the third-order structure function $\langle \Delta u_r^3 \rangle$. Using a similar reasoning it can be shown that in the inertial range $[2^{-\alpha_{\max}} \le r \le (1-s)2^{-\alpha_{\min}}]$, the third-order structure function is

$$\frac{\langle \Delta u^3 \rangle}{U_0^3 \langle V^2 \rangle^{3/2} \gamma\left[\frac{r}{\sqrt{2\pi}}\right]}=\left[\frac{r}{2^{-\alpha_{\min}}}\right]^3\frac{1-2s}{2s^2(1-s)^2}+\left[\frac{r}{2^{-\alpha_{\min}}}\right]^4\frac{\left[\frac{2+s}{s^3}-\frac{3-s}{(1-s)^3}\right]}{12}+\left[\frac{r}{2^{-\alpha_{\min}}}\right]g(s) \tag{A15}$$

for $2^{-\alpha_{\max}} \le r \le (1-s)2^{-\alpha_{\min}}$ and

$$g(s)=\frac{1-2s}{2s^2}-\left[\frac{2+s}{s^3}-\frac{3-s}{(1-s)^3}\right]\frac{(1-s)^3}{12}-\frac{s^3-(1-s)^3}{6s^3}$$
$$+\frac{3(2s-1)}{2s^2}-\frac{\ln[s/(1-s)]}{s^2}+\frac{(1+s)(2s-1)}{4s^3}+\frac{1-2s}{4s^3(1-s)}$$
$$+\frac{(1-2s)\ln(s)}{s^2(1-s)^2}+\frac{3(1-2s)}{2s^2(1-s)}-\frac{(1-2s)(1+s)}{2s^2(1-s)}+\frac{(1-2s)(1-s^3)}{12s^2(1-s)^2}\ .$$

[1] K. R. Sreenivasan and A. Juneja (unpublished).
[2] B. B. Mandelbrot and J. W. Van Ness, SIAM Rev. **10**, 422 (1968).
[3] A. N. Kolmogorov, Dokl. Akad. Nauk SSSR **32**, 16 (1941).
[4] J. Eggers and S. Grossmann, Phys. Rev. A **45**, 2360 (1992).
[5] J. A. C. Humphrey, C. A. Schuler, and B. Rubinsky, Fluid Dyn. Res. **9**, 81 (1992).
[6] T. Vicsek and A. L. Barabasi, J. Phys. A **24**, L485 (1991).
[7] R. Benzi, L. Biferale, A. Crisanti, G. Paladin, M. Vergassola, and A. Vulpiani, Physica D **65**, 352 (1993).
[8] B. B. Mandelbrot, J. Fluid Mech. **62**, 331 (1974).
[9] C. Meneveau and K. R. Sreenivasan, J. Fluid Mech. **224**, 429 (1991).
[10] A. B. Chhabra and K. R. Sreenivasan, Phys. Rev. Lett. **68**, 2762 (1992); multiplier distributions in other contexts have also been considered by A. Erzan, S. Grossmann, and A. Hernandez-Machado, J. Phys. A **20**, 3913 (1987).
[11] K. R. Sreenivasan and G. Stolovitzky, Acta Mech. Suppl. **4**, 113 (1994).
[12] C. Meneveau and K. R. Sreenivasan, Phys. Rev. Lett. **59**, 1424 (1987).
[13] A. Chhabra, R. V. Jensen, and K. R. Sreenivasan, Phys. Rev. A **40**, 4593 (1989).
[14] A. N. Kolmogorov, J. Fluid Mech. **13**, 82 (1962).
[15] G. Stolovitzky, P. Kailasnath, and K. R. Sreenivasan, Phys. Rev. Lett. **69**, 1178 (1992); S. G. Thoroddsen and C. W. Van Atta, Phys. Fluids A **4**, 2592 (1992); A. Praskovsky, *ibid.* **4**, 2596 (1992); D. Lohse and S. Grossmann, Physica A **194**, 519 (1993).
[16] G. K. Batchelor, *The Theory of Homogeneous Turbulence* (Cambridge University Press, Cambridge, England), Chap. 6; K. R. Sreenivasan, Phys. Fluids **27**, 1048 (1984). In fact, experiments show that A depends on the Reynolds number Re for moderate values of Re, but tends to a constant close to unity for high enough Re.
[17] B. Castaing, Y. Gagne, and E. J. Hopfinger, Physica D **46**, 177 (1990).
[18] R. F. Voss, Physica D **38**, 362 (1989).
[19] J. Feder, *Fractals* (Plenum, New York, 1988).
[20] P. Kailasnath, K. R. Sreenivasan, and G. Stolovitzky, Phys. Rev. Lett. **68**, 2766 (1992); S. Grossmann and D. Lohse, Europhys. Lett. **21**, 201 (1993).
[21] G. I. Taylor, Proc. R. Soc. London Ser. A **151**, 421 (1935).
[22] C. Meneveau and K. R. Sreenivasan, Nucl. Phys. B (Proc. Suppl.) **2**, 49 (1987).
[23] L. Zubair, Ph.D. thesis, Yale University, 1993.
[24] B. Dubuc, J. F. Quiniou, C. Roques-Carmes, C. Tricot, and S. W. Zucker, Phys. Rev. A **39**, 1500 (1989).
[25] K. R. Sreenivasan and P. Kailasnath, Phys. Fluids A **5**, 512 (1993).